Applied Catalysis B: Environmental 111–112 (2012) 317–325

Contents lists available at SciVerse ScienceDirect

Applied Catalysis B: Environmental

journal homepage: www.elsevier.com/locate/apcatb

# Boosting the electrocatalytic activities of $SnO_2$ electrodes for remediation of aqueous pollutants by doping with various metals

So Young Yang[a], Yeon Sik Choo[a], Soonhyun Kim[b], Sang Kyoo Lim[b], Jaesang Lee[c], Hyunwoong Park[d,*]

[a] Department of Biology, Kyungpook National University, Daegu 702-701, Republic of Korea
[b] Division of Nano-Bio Technology, Daegu Gyeongbuk Institute of Science and Technology, Daegu 704-230, Republic of Korea
[c] Water Research Center, Korea Institute of Science and Technology, Seoul 136-791, Republic of Korea
[d] School of Energy Engineering, Kyungpook National University, Daegu 702-701, Republic of Korea

ARTICLE INFO

*Article history:*
Received 28 June 2011
Received in revised form 8 October 2011
Accepted 11 October 2011
Available online 17 October 2011

*Keywords:*
Electrocatalytic
Water treatment
Antimony
Sb–$SnO_2$
Doping

ABSTRACT

The purpose of this study is to search for effective dopants and their optimal combinations to improve the electrocatalytic activity of the $SnO_2$ electrode for the remediation of aqueous pollutants. For this purpose, Sb was selected as the primary dopant for $SnO_2$ and six elements (Fe(III), Ni(II), Co(II), Ru(III), Ce(III), and Pd(II)) were also introduced into the optimized Sb–$SnO_2$ electrodes. The electrodes were checked for their electrochemical properties at different doping levels and tested for their electrocatalytic activities for the degradation of phenol and Eosin Y. In addition, RNO (N,N-dimethyl-p-nitrosoaniline) was used as a probe molecule for OH radicals to examine the reaction mechanism occurring at the electrodes. Sb with a 5–10 at.% was most effective in making $SnO_2$ an electrocatalyst and Ni (~1%) enhanced the degradation rate and TOC removal rate of phenol at the Sb–$SnO_2$ anode by a factor of 14 and 8, respectively. Fe also increased the activity moderately. Enhanced Ni–Sb–$SnO_2$ activity was also found for Eosin Y. The other co-dopants exhibited various degrees of positive or negative effects depending on the substrate. The lack of a correlation in the kinetics between substrate degradation and the RNO changes indicated that the primary electrocatalytic reactions may proceed via direct electron transfer and/or organic peroxy radical-mediation, not OH radical-mediation. Detailed analyses of the electrode surfaces (SEM, TEM, XRD, and XPS) and quantification of intermediates were carried out to obtain insight into the heterogeneous electrocatalytic reaction.



## 1. Introduction

As diverse and recalcitrant aqueous pollutants have been discharged and more stringent environmental regulations have been implemented, electrochemically advanced oxidation processes (EAOPs) have attracted increasing attention as a viable alternative to conventional treatment processes [1–5]. EAOPs have several advantages over conventional ones including simple setup of the electrode couple (anode and cathode), relatively easy and cost-effective fabrication of electrodes, and mineralization of most aqueous pollutants at ambient temperature and pressure. The efficiency of EAOPs depends strongly on the type of anode and electrolyte, and applied power (current and voltage), among which the anode is the most critical component because of the initiation of the overall electrochemical process on its surface [9]. To date, a range of anodes were investigated, such as platinum [3,6,7], dimensionally stable anodes ($IrO_2$ [8], $RuO_2$ [4,6,8,9]), $SnO_2$ [7,10], $PbO_2$ [11,12], Nb–$TiO_2$ [13], Bi–$TiO_2$ [14–17], and boron-doped diamond [2,11,18].

Among them, $SnO_2$ has been studied extensively due to the low cost of materials and fabrication. $SnO_2$ is a type of wide-bandgap ($E_g$) semiconductor with an $E_g$ of 3.6 eV, and is often doped to reduce the bandgap and increase the electric conductivity. Several elements (e.g., Sb, Ar, F, B, Cl, and P) were doped [5,19], among which Sb was found to be the most effective in enhancing the electrocatalytic activity of $SnO_2$ [19,20]. Sb–$SnO_2$ has a high oxygen evolution potential and generates hydroxyl radicals more effectively than the anodes of low oxygen evolution potentials (e.g., $RuO_2$) [9], achieving the cold combustion of substrates via an indirect (mediated) oxidation pathway.

Recently, various co-dopants were introduced to Sb–$SnO_2$ to further enhance the electrocatalytic activity, improve the stability, and identify novel functionalities. The Fe(III)-doped Sb–$SnO_2$ anode was reported to have a maximum 3-fold enhanced activity for the degradation of phenolic compounds primarily

* Corresponding author. Tel.: +82 53 950 7371; fax: +82 53 952 1739.
*E-mail address:* hwp@knu.ac.kr (H. Park).

0926-3373/$ – see front matter © 2011 Elsevier B.V. All rights reserved.
doi:10.1016/j.apcatb.2011.10.014

because of the enhanced adsorption of the substrates and charge compensation by ferric ions [21]. Rare earth elements (Ce, Eu, Gd, and Dy) also were used as dopants; Ce was found to adversely affect the electrocatalytic activity of Sb–$SnO_2$ for phenol [22,23]. On the other hand, Ce-doped Sb–$SnO_2$ had a better activity than Sb–$SnO_2$ for the degradation of an aqueous dye (Orange II) [24]. Ruthenium was also considered a co-dopant [4,25] but there was no comparison of the electrocatalytic activity between Sb–$SnO_2$ and Ru–Sb–$SnO_2$ in treating contaminated water. Nickel was reported to facilitate the electrocatalytic generation of ozone at Sb–$SnO_2$ [26] and enhance the electrochemical degradation of phenol [27] and 4-chlorophenol [28].

This study evaluated effective dopants and their optimal combinations for improving the electrocatalytic activity of the $SnO_2$ anode, as well as a quantitative comparison of the dopant effects. For this purpose, Sb was selected as the first dopant for $SnO_2$ and six elements (Fe(III), Ni(II), Co(II), Ru(III), Ce(III), and Pd(II)) were also introduced into the optimized Sb–$SnO_2$ electrode. The electrodes were examined for their electrochemical properties at different doping levels, and the electrocatalytic activities for degradation of phenol and Eosin Y were compared. In addition, RNO (N,N-dimethyl-p-nitrosoaniline) was used as a probe molecule for OH radicals to examine the reaction mechanism occurring at the electrodes.

## 2. Experimental

### 2.1. Reagents and electrode preparation

$SnCl_4{\cdot}5H_2O$ (98%, Aldrich), $SbCl_3$ (99%, Aldrich), $FeCl_3{\cdot}6H_2O$ (98%, Aldrich), $NiCl_2{\cdot}6H_2O$ (>reagent grade, Aldrich), $CoCl_2{\cdot}6H_2O$ (98%, Aldrich), $RuCl_3{\cdot}xH_2O$ (>reagent grade, Aldrich), $CeCl_3{\cdot}7H_2O$ (99.9%, Aldrich), and $PdCl_2$ (99%, Dae-Jung) were used as received. Phenol (PhOH: 99%, Aldrich), Eosin Y (EY: 85%, Dae-Jung), N,N-dimethyl-4-nitrosoaniline (RNO: 97%, Aldrich) were used without any purification. 1,3,5-Trihydroxybenzene (THB: 97%, Aldrich), hydroquinone (HQ: 99%, Aldrich), resorcinol (RC: 99%, Aldrich) and catechol (CC: 99%, Aldrich) were used for intermediate analysis. $Na_2SO_4$ (99%, Dae-Jung) was employed as the supporting electrolyte reagent.

To prepare the Sb-doped $SnO_2$ electrodes, a titanium mat (0.127 mm thick, 99.7%-pure, Aldrich) was cut into small foils with size of 15 mm × 30 mm, which were polished with sand paper (400-grid) and etched in a c-HCl solution for 10 min, followed by washing with distilled water. The pretreated titanium foils were dipped 5 times into a coating solution containing Sn(IV) (0.1 mM) and Sb(III) (0.1 mM) at varying atomic ratios (Sb/(Sn + Sb)) of 0–100%. After drying under ambient conditions, the foils were annealed at 450 °C for 5 min under air. This dipping-annealing cycle was repeated 10 times. In the final stage, the foil was annealed at 450 °C for 1 h. For co-doped $SnO_2$ anodes, the coating solutions of Sn(IV) and Sb(III) (Sn:Sb = 95:5) including Fe(III), Ni(II), Co(II), Ru(III), Ce(III), or Pd(II) with varying at.% (M/(Sn + Sb + M) where M refers to co-dopants) were prepared, and the above dipping-coating procedure was repeated. EDX analysis indicated that the M(0.5%)–Sb(5%)–$SnO_2$ electrodes had a surface composition of Sb and M of 7.06–13.6% and 3.13–4.85%, respectively (Table S1 in Supporting Material). On the other hand, XPS showed that Ni(0.5%)–Sb(5%)–$SnO_2$ electrodes had surface composition of Sb 4.3% and Ni 0.4%, which is consistent with the solution composition. Different analytic techniques result in different surface composition ratios due to the different measurement principles and measurement depth or area. In some cases, surface enrichment and segregation of dopants can cause deviation.

### 2.2. Electrochemical measurements

The electrochemical properties of the as-prepared electrodes were analyzed by cyclic voltammetry (CV) using a potentionstat (Versastat 3-400, Princeton Applied Research). The electrodes with a saturated calomel electrode (SCE, reference electrode) and a graphite rod (counter electrode) were placed in an aqueous electrolyte of 0.1 M $Na_2SO_4$ and the potentials were applied with a sweep rate of 0.1 V/s from −0.5 to +2.5 V vs. SCE. For the electrocatalytic activities of the electrodes, the electrochemical reactions were conducted with an anode–cathode couple immersed in a 20-mL aqueous solution containing 0.1 M $Na_2SO_4$ as a supporting electrolyte and a single substrate (0.1 mM or 0.8 mM phenol (PhOH), 1 mM Eosin Y (EY), or 1 mM RNO). The electrode couple was composed of a single anode (Sb–$SnO_2$ or M–Sb–$SnO_2$) with an active area of 4.5 $cm^2$ (1.5 cm × 1.5 cm, both sides) in contact with the solution and two plates of a same-size stainless steel (SS) cathode that faced both sides of the anode with a separation of 3 mm. A constant cell voltage ($E_{cell}$) or cell current ($I_{cell}$) was applied to the electrode couple with a DC-power supply (E3633A, Agilent).

The time-profiled changes in phenol and its intermediates were analyzed by high performance liquid chromatography (HPLC, YL9100) equipped with a C18 column (Thermo). The HPLC eluent was composed of 55 vol.% distilled water (0.1 vol.% phosphoric acid included) and 45 vol.% acetonitrile at a flow rate of 1 mL/min. A total organic carbon (TOC) analyzer (TOC-5000A, Shimadzu) was used to assess the degree of mineralization of phenol. The Eosin Y and RNO concentrations [29] were determined by recording their main absorption bands at 517 and 440 nm, respectively, using a UV–vis spectrophotometer (Perkin Elmer, Lambda 950).

### 2.3. Surface characterization

The morphology of the as-prepared electrodes was examined by field emission scanning electron microscopy (FE-SEM, Hitachi S-4800) with an energy-dispersive X-ray spectroscope (EDX) and scanning transmission electron microscope (STEM; Hitachi, HD-2300). X-ray diffraction (XRD, Rigaku D/Max-2500) and X-ray photoelectron spectroscopy (XPS, VG scientific, ESCA LAB 220i XL, MgK( source) were used to examine the crystalline patterns of the electrodes and the binding energies of their elements, respectively.

## 3. Results and discussion

### 3.1. Electrode surface characterizations

Fig. 1 shows SEM images of Sb–$SnO_2$ (Sb 5%) and M–Sb–$SnO_2$ (M = Ni, Ce, and Fe with each 0.5%) electrode surfaces. Overall, the surface morphology had the high-porous micro-structures created by aggregated particles, and each aggregated one was composed of many spherical particles with a size of approximately 20 nm. It seemed that metal doping did not significantly affect the primary particle sizes of electrocatalysts. For more accurate determination of the particle sizes, the particles formed on base Ti metals were collected as powders, dispersed (in ethanol) in an ultrasound bath, and analyzed with a scanning TEM (STEM). It has been found that even though the particles were aggregated the size of discrete particles could be estimated to be around 10–20 nm in diameter (Fig. 2). Ni and Ce doping little affected the particle size of Sb–$SnO_2$ whereas Fe doping increased the size by ca. 2–3 nm. The oxide surfaces were also examined by XRD to check their crystalline characteristics (Fig. 3). Similarly to a previous study [9], Sb–$SnO_2$ and M–Sb–$SnO_2$ had only $SnO_2$-originated oxide peaks (26°, 34°, and 52° 2$\theta$) without any signs of Sb-related (e.g., $Sb_2O_5$) or M-related oxides. No

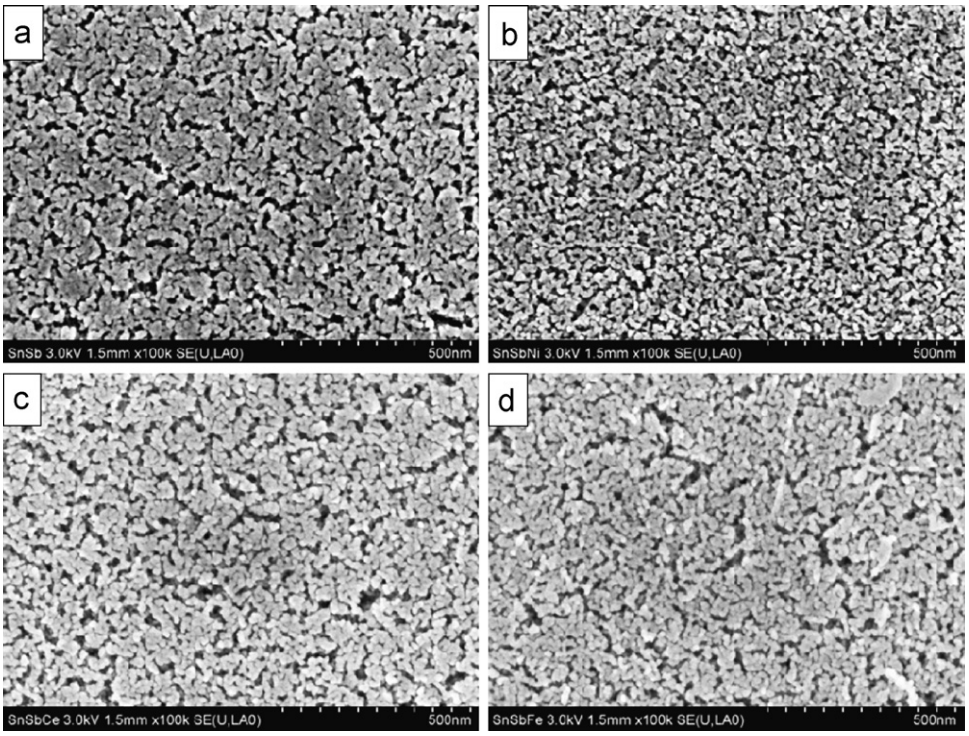


**Fig. 1.** SEM images of (a) Sb–$SnO_2$, (b) Ni–Sb–$SnO_2$, (c) Ce–Sb–$SnO_2$, and (d) Fe–Sb–$SnO_2$. Sb and other metals (M) were doped at 5% and 0.5%, respectively.

signs for those peaks result likely from their mixing with the $SnO_2$ structure and low doping level [22].

XPS was also conducted to verify the existence of dopants at Ni–Sb–$SnO_2$ (i.e., Sb and Ni), illuminate their chemical valence, and examine how metal-doping affects the chemical bonding status of $SnO_2$. The overall survey patterns (in particular for Sn, O, and Sb) were similar. The valence state of Sn was determined to be +4 in the form of $SnO_2$ (Sn 3d5/2 at 487.1 eV and 3d3/2 at 495.5 eV) (Fig. S1 in Supporting Material). No chemical shift of the Sn band was observed by Sb and/or Ni doping, indicating that these dopants did not significantly affect the electronic structure of $SnO_2$. In addition, the valence state of Sb was determined to be +5 in the form of $Sb_2O_5$ (Sb 3d3/2 at 540.5 eV) (Fig. 4a) [28,30], suggesting that annealing might oxidize $Sb^{3+}$ to $Sb^{5+}$. In some cases, $Sb^{3+}$ located

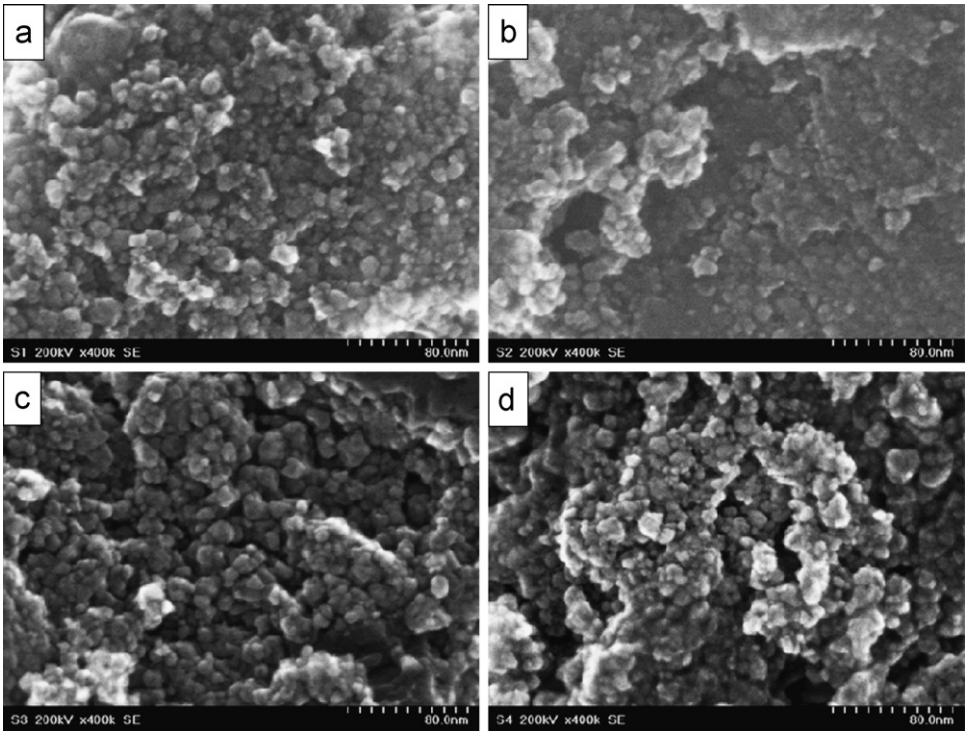


**Fig. 2.** Scanning TEM images of (a) Sb–$SnO_2$, (b) Ni–Sb–$SnO_2$, (c) Fe–Sb–$SnO_2$, and (d) Ce–Sb–$SnO_2$. Sb and other metals (M) were doped at 5% and 0.5%, respectively.

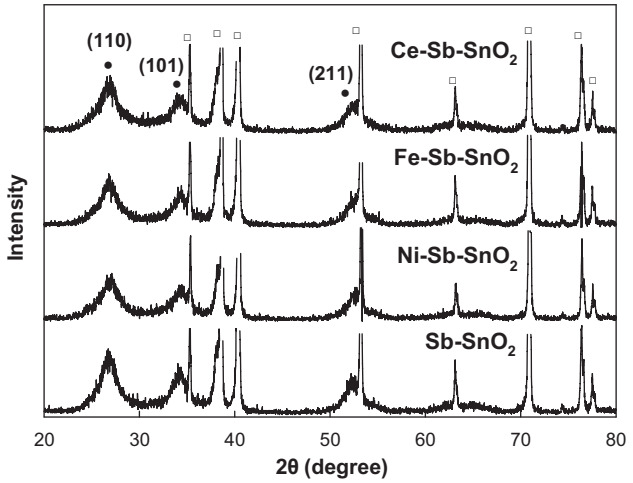


**Fig. 3.** XRD patterns of Sb–$SnO_2$ and Ni-, Fe- and Ce-doped Sb–$SnO_2$. ● $SnO_2$, □ Ti (from base material). Sb and other metals were doped at 5% and 0.5%, respectively.

at ca. 539.2 eV was also observed by resolving the Sb 3d3/2 band, but the amount was quite low compared to $Sb^{5+}$ [31,32]. Ni doping did not affect the chemical shift of Sb 3d3/2 but it shifted a band at 531.1 eV by 0.2 eV to a lower energy. This band was assigned as a mixed band with Sb 3d5/2 and O 1s. Therefore, the lack of a shift in Sb 3d3/2 by Ni doping suggests that the 0.2 eV-shift of the band centered at 531.1 eV should be related to O 1s not to Sb 3d5/2. To gain insight into the hidden O 1s and Sb 3d5/2, the band was deconvoluted by fixing the Sb 3d5/2 band (532.6 eV) with an intensity ratio of 1.44 for Sb 3d5/2-to-Sb 3d3/2 (Fig. 4b and c). Two O 1s bands located at 533.1 eV and 531.2 eV were obtained from the deconvolution; the former is likely to be associated with metal hydroxides (Sn–OH) or hydrated species [31], whereas the latter may originate from metallic oxides ($SnO_2$). The former oxygen is likely to actively participate in redox chemistry and protonation/deprotonation occurring at the electrode/water interface, and hence it is involved in the generation of active oxygen species in the electrocatalysis and plays a key role in electrocatalytic oxidation [22]. A comparison of the areas for the O 1s band (533.1 eV) between Sb–$SnO_2$ and Ni–Sb–$SnO_2$ indicated that Ni doping increased the area by ~5%, which suggests that Ni doping may enhance the electrocatalytic activity of Sb–$SnO_2$. Finally, a band for Ni 3p3/2 was observed at 856.3 eV (Fig. 4d), indicating that Ni exists as Ni(II) in the form of NiO and/or $Ni(OH)_2$.

### 3.2. Optimization for electrocatalytic activities

Before synthesizing the M–Sb–$SnO_2$ electrodes, the optimal doping level of Sb was examined by varying the Sb/(Sn + Sb) ratios of the coating solution from 0 to 100%. Fig. 5a shows the representative cyclic voltammetry (CV) plots of the Sb–$SnO_2$ electrodes in 0.1 M $Na_2SO_4$ (for complete set of CVs, see Fig. S2). Obviously, $SnO_2$ without Sb (Sn 100%; line A) had no activity in generating a current in the potential range of −0.5 V vs. SCE to +2.5 V vs. SCE primarily because of its wide bandgap (3.6 eV) and low electric conductivity [5,6,9,19,33]. On the other hand, Sb doping at 5% (line B) enhanced anodic current generation significantly from at 1.7 V vs. SCE. Heavier doping with 20% (line C) marginally decreased it and 100% Sb (i.e., $Sb_2O_5$; line D) lost the activity completely. Therefore, plotting the anodic currents measured at 2.0 and 2.3 V vs. SCE as a function of the Sb doping level resulted in volcano-shaped curves

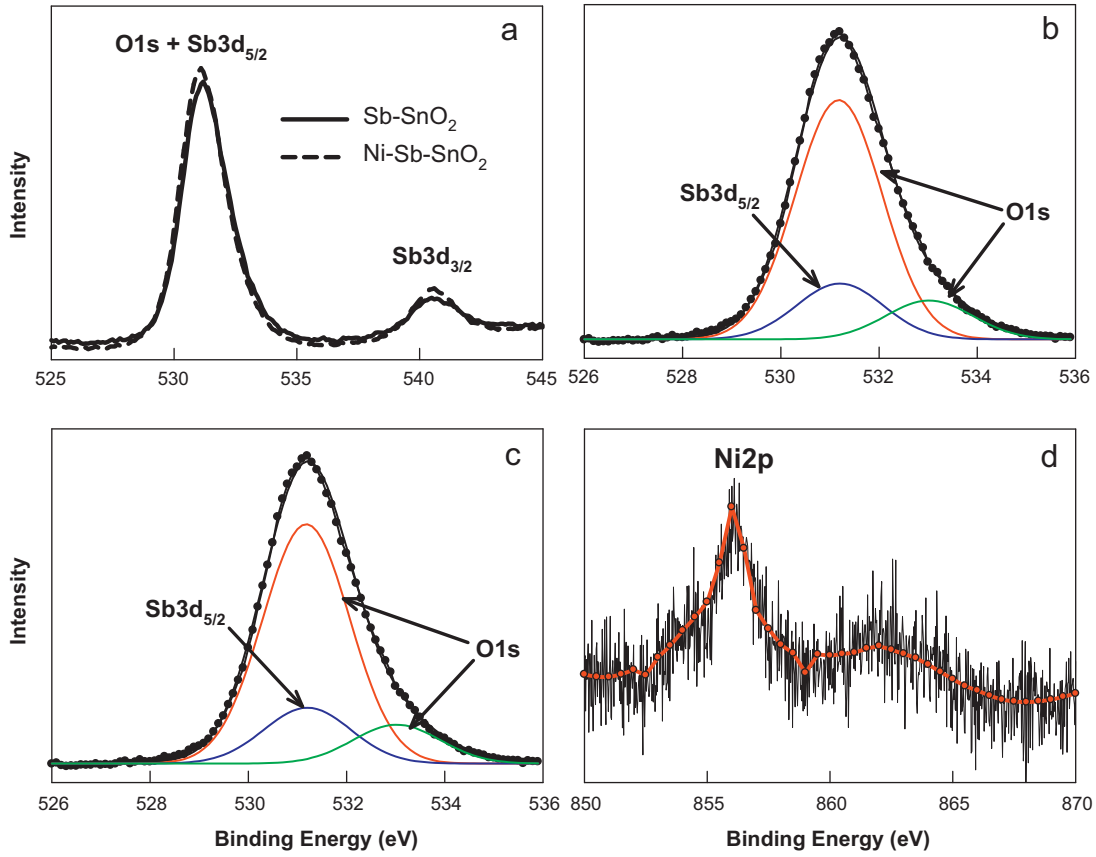


**Fig. 4.** (a) XPS spectra of O1s and Sb3d bands for Sb–$SnO_2$ and Ni–Sb–$SnO_2$. (b and c) Deconvoluted XPS spectra of O1s and Sb3d5/2 mixed bands (531.2 eV) for (b) Sb–$SnO_2$ and (c) Ni–Sb–$SnO_2$. (d) XPS spectrum of Ni2p at Ni–Sb–$SnO_2$. Sb and Ni were doped at 5% and 0.5%, respectively.

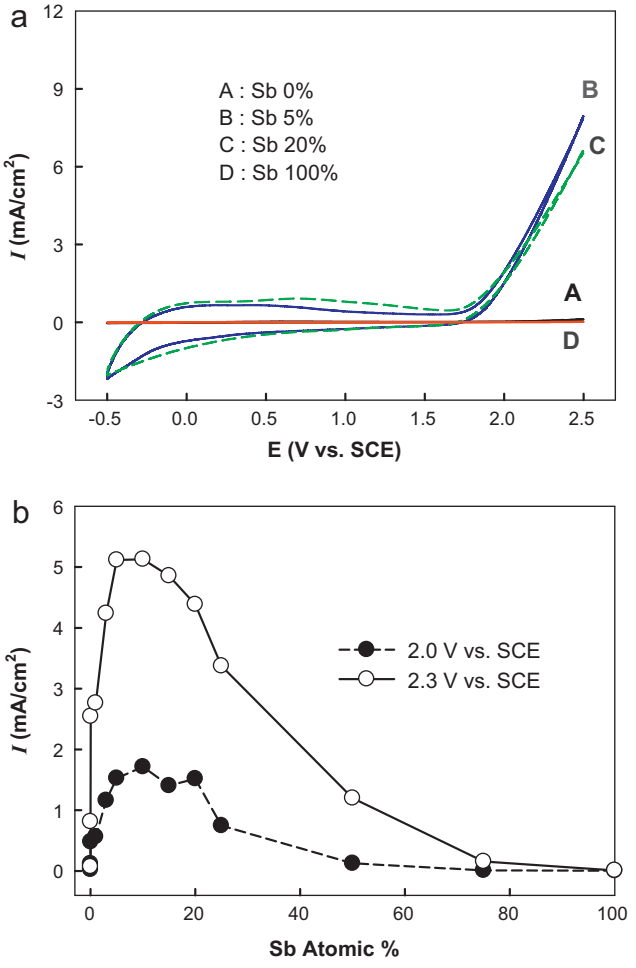


**Fig. 5.** Sb doping effects on (a) cyclic voltammograms of Sb–$SnO_2$ and (b) current generations of Sb–$SnO_2$ at 2.0 V and 2.3 V vs. SCE in 0.1 M $Na_2SO_4$ electrolyte.

with the most optimal range of 5–10% (Fig. 5b). The existence of the optimal doping level suggests that at a lower doping level, Sb might reduce the resistivity of $SnO_2$ by increasing the extra charge carriers and enhance the mobility of these charge carriers by improving the crystallinity of $SnO_2$ [19,33–35]. On the other hand, at a higher doping level, the resistivity of $SnO_2$ is likely to increase with decreasing crystallinity of $SnO_2$ [19,34]. Furthermore, some part of Sb can exist as Sb(III) at a heavy doping level, leading to charge recombination between Sb(III) and Sb(V) [34], thereby reducing the cell current.

To further improve the electrocatalytic effect of $SnO_2$, a range of metals, such as Fe(III), Ni(II), Co(II), Ru(III), Ce(III), and Pd(II), were doped at various at.% (0.5–5%) into Sb(5%)–$SnO_2$ electrodes and their CVs were compared (see Fig. S3). The electrochemical behaviors depend strongly on the doping level. For example, an increase in the Ni doping level from 0.5% to 5% affects the overall CV patterns of Sb–$SnO_2$ only marginally (Fig. 6a), whereas Fe and Ce doping reduces the anodic current generation of Sb–$SnO_2$ significantly at $E >$ ca. 1.7 V vs. SCE (Fig. 6b and c). In particular, Ce doping at 5% caused no redox behavior of Sb–$SnO_2$, making it completely inert to the applied voltage (i.e., degenerated). At a doping level of 0.5–2%, Ce–Sb–$SnO_2$ had two current peaks at ca. 1.1 V vs. SCE of the anodic scan and 0.75 V vs. SCE of the cathodic scan resulting from $Ce^{4+}/Ce^{3+}$ redox reaction [22]. On the other hand, Ru and Pd increased the anodic currents with increasing doping levels (Fig. S3). The CV data of the M(0.5%)–Sb(5%)–$SnO_2$ electrodes were shown together for a quantitative comparison (Fig. 6d). Ru and Pd enhanced current generation along with cathodic shifts in the current-onset potential (i.e., oxygen evolution potential) by 0.2–0.3 V. Such lowered oxygen evolution potentials suggest that Ru- and Pd-doped Sb–$SnO_2$ may have a more pronounced direct electrochemical reaction. These dopants are likely to alter the surface properties of Sb–$SnO_2$ (e.g., concentration of oxygen vacancies in the $SnO_2$ lattice) influencing its electrocatalytic performance [36] particularly for cathodic hydrogen production (particularly Pd; Fig. S3).

To examine the electrocatalytic activities, M–Sb–$SnO_2$ electrodes (anodes) were coupled with stainless steels (cathodes) and a constant anodic current of 0.1 A was applied to the couples in 0.1 M $Na_2SO_4$ electrolyte containing 1 mM Eosin Y (EY) or 0.1 mM phenol as a model substrate. As shown in Fig. 7a, the pseudo first order decay rate of EY at Sb–$SnO_2$ was estimated to be 0.009 $min^{-1}$, which was enhanced by Fe, Pd, Ni, Ru, and Co doping at 0.5% by a factor of 30–200%. In particular, the Ni effect was most significant with doping at 1–2% (Fig. 7b and Fig. S4). In the case of phenol (Fig. 7c), its pseudo first order decay rate at Sb–$SnO_2$ was determined to be 0.03 $min^{-1}$, and Ru and Pd reduced the rate slightly to 0.021 and 0.022 $min^{-1}$, respectively. Ce did not affect the rate, which is similar to a previous report that Ce doping reduced the rate of phenol degradation marginally (~12%) [22]. Fe enhanced the rate moderately by approximately 1.5 times, the effect of which is slightly lower than the reported one [21]. Similarly to the case of EY, Ni doping at 0.5 at.% enhanced the rate of phenol degradation by more than 8-fold and the enhancements were more pronounced with increasing Ni doping level (14.1 times at 1% and 13.5 times at 2%) (Fig. 7d). Heavier doping at 5–7% resulted in slightly reduced electrocatalytic activity but the effect of Ni was still maintained. The role of Ni in this study seems to be multiple. The Ni dopant might improve the binding affinity of oxygen at the electrode surface, as indicated by the increase in the area of the O 1s (533.1 eV). Ni also might affect the electrical conductivity of Sb–$SnO_2$. For example, the electrical conductivity of Sb–$SnO_2$ can be decreased at a higher doping level of Ni (≥5%) [28] and thus the electrocatalytic activity for phenol appeared to be reduced. Finally, Ni can enhance the generation of reactive oxygen species such as ozone ($O_3$), hydroxyl radicals (•OH) and hydroperoxy radicals (•OOH). It was reported that Ni doping increased the electrolytic generation of ozone at Sb–$SnO_2$ anode by ~33% in the acidic electrolytes ($H_2SO_4$, $HClO_4$, and $H_3PO_4$) [26,28]. This study used the different electrolyte ($Na_2SO_4$) and pH (5–7), yet ozone could be still involved to the electrocatalytic reaction directly or indirectly. If ozone is involved, then other radicals can be involved too because they are the products or precursors of ozone (see next section for discussion).

Fig. 8a compares the time-profiled concentration changes in phenol and intermediates between Sb(5%)–$SnO_2$ and Ni(0.5%)–Sb(5%)–$SnO_2$ anodes in 0.1 M $Na_2SO_4$ electrolyte. When Sb–$SnO_2$ anode was used, a range of mono-hydroxylated intermediates (catechol (CC), resorcinol (RC), and hydroquinone (HQ)) and a di-hyroxylated one (1,3,5-trihydroxybenzene, THB) were observed in the range of 5–40 μM. The existence of these hydroxylated intermediates suggests that the phenol degradation was likely to proceed via reactions with hydroxyl radicals. On the other hand, the electrochemical reaction of phenol at the Ni–Sb–$SnO_2$ anode produced only a small amount of THB (~3 μM) without mono-hydroxylated ones. This suggests that (1) the primary mechanism for the degradation of phenol is changed from a hydroxyl radical-mediated reaction (indirect, bulk oxidation) to direct electron transfer reaction (direct, surface reaction) and/or (2) that the degradation kinetics of phenol is accelerated so much that the intermediates may not be detected in the time scale of this study (see the next section for discussion). Fig. 8b shows the time-profiles of TOC changes during the reactions of phenol in Fig. 8a. In 1 h-electrolysis, the TOC for Sb–$SnO_2$ anode was decreased by 20%, whereas that for Ni(0.5%)–Sb–$SnO_2$ had a TOC change of ca. 55%. In the prolonged reactions for 2.5 h, the TOC

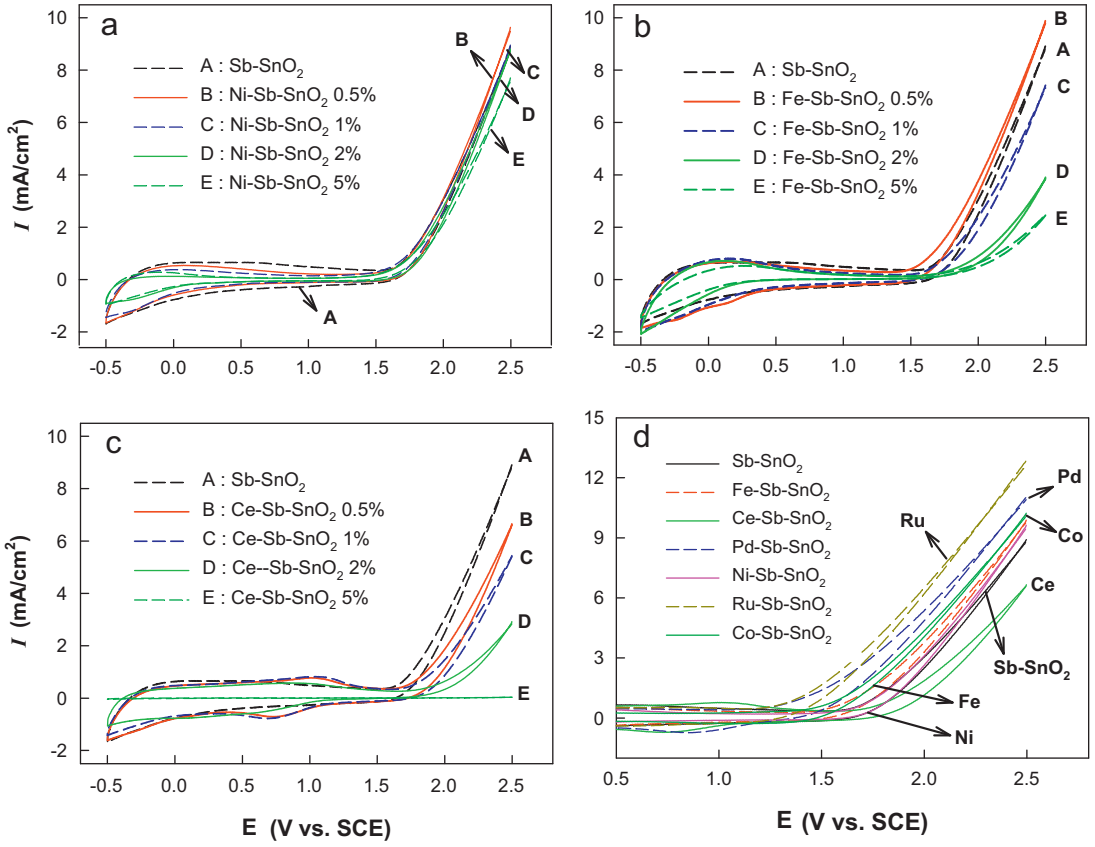


**Fig. 6.** (a–c) Effects of doping levels (0–5%) on the electrochemical behaviors of (a) Ni–Sb–$SnO_2$, (b) Fe–Sb–$SnO_2$, (c) Ce–Sb–$SnO_2$. (d) Comparison of Sb–$SnO_2$ and M(0.5%)–Sb–$SnO_2$ for their electrochemical behaviors. Sb-doped at 5%.

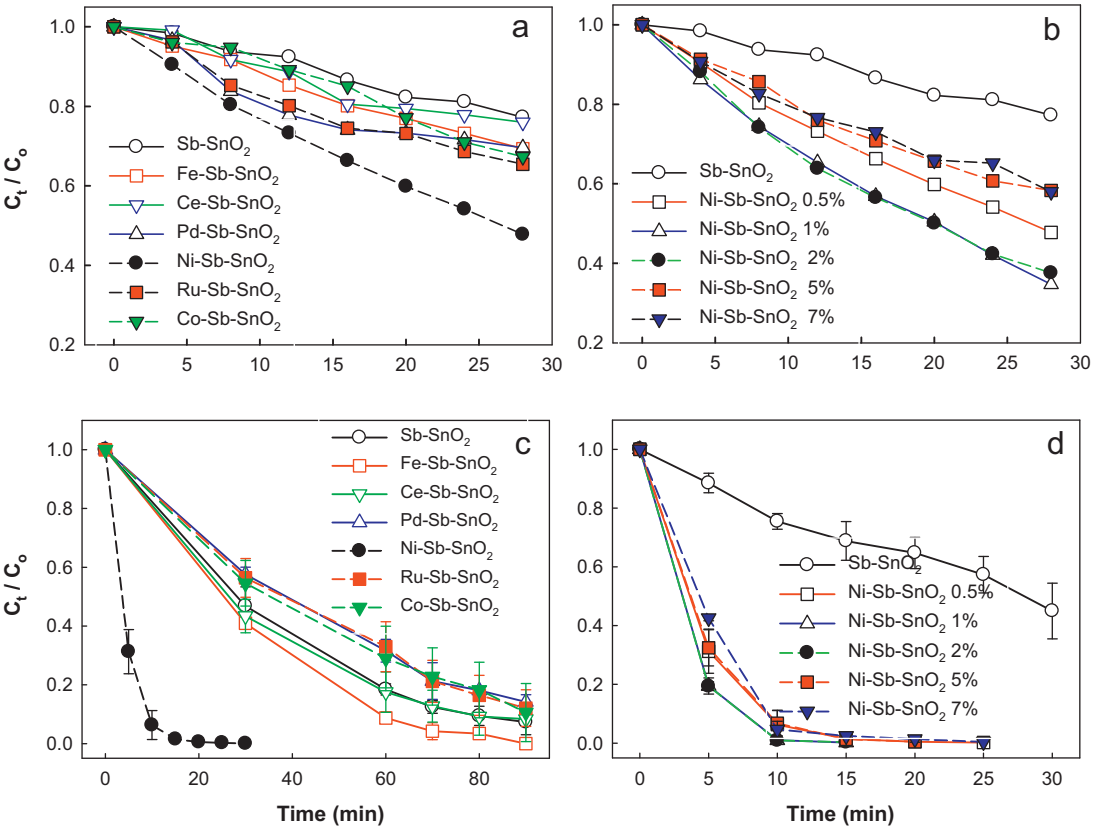


**Fig. 7.** Time-profiled concentration changes of (a and b) Eosin Y and (c and d) phenol at (a and c) M(0.5%)–Sb(5%)–$SnO_2$ and (b and d) Ni–Sb(5%)–$SnO_2$ anodes with varying Ni doping %. $[Eosin\ Y]_0 = 1$ mM; $[phenol]_0 = 0.1$ mM; $I = 0.1$ A; 0.1 M $Na_2SO_4$.

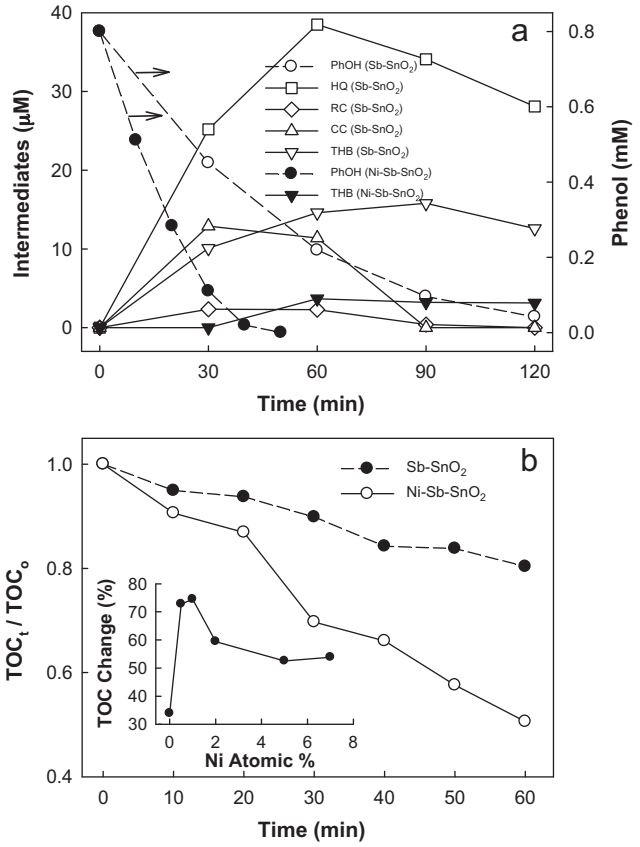


**Fig. 8.** Time-profiled changes of (a) phenol and intermediates and (b) TOC in the degradation of phenol at Sb(5%)–$SnO_2$ and Ni(0.5%)–Sb(5%)–$SnO_2$ anodes. Inset shows the TOC changes after 150 min-electrolysis. $I$ = 0.1 A; $[phenol]_0$ = 0.8 mM; 0.1 M $Na_2SO_4$. PhOH, phenol; HQ, hydroquinone; RC, resorcinol; CC, catechol; THB, 1,3,5-trihydroxybenzene.

change for Ni(0.5%)–Sb–$SnO_2$ increased to ~75%, whereas an increase in the Ni doping level to 7% decreased the TOC gradually to ~50% (Fig. 8b inset). To compare the electrocatalytic efficiencies of Sb–$SnO_2$ and Ni–Sb–$SnO_2$ quantitatively, the TOC removal index (mg-Carbon/Coulombs) was introduced with the following definition:

$$\text{TOC removal index} = \frac{(\text{TOC}_t - \text{TOC}_{t+\Delta t}) \times V}{I \times \Delta t} \quad (1)$$

where TOC is the total organic carbon (mg-carbon/L), $V$ is the volume of electrolyte (L), $I$ is the current (A), and $\Delta t$ is the time change (s). The indices of Sb–$SnO_2$ and Ni–Sb–$SnO_2$ started with ca. 1.5 and 7.7, respectively, decreasing gradually with electrolysis time (Fig. S6). Higher index values of Ni–Sb–$SnO_2$ at the initial phase can be attributed to enhanced direct oxidation (pathway 1 in Scheme 1) and/or the more efficient generation of reactive species (e.g., hydroxyl radicals: pathways 2 and 3). The latter might result from the weaker adsorption of the reactive species at the electrode surface. The decreases in indices at the prolonged phase are due likely to the generation of more recalcitrant intermediates, such as aliphatic acids. The recalcitrance of aliphatic acids might also reduce the efficiency for the direct oxidation performance of the anodes.

### 3.3. Electrocatalytic reaction mechanism

To determine if radical species are involved in the electrocatalytic degradation of substrates, the reactions of RNO, a hydroxyl radical quencher, at Sb–$SnO_2$ and M–Sb–$SnO_2$ anodes, were investigated by monitoring its optical change at 440 nm [29,38]. As

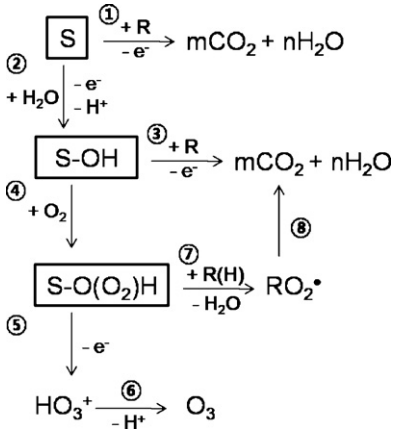


**Scheme 1.** Proposed electrocatalytic reaction mechanism for degradation of substrate (R and RH). S refers to anode surface.

shown in Fig. 9a, all anodes except Ni–Sb–$SnO_2$ had lower activities for RNO than Sb–$SnO_2$. In the case of Ni–Sb–$SnO_2$, there was an approximately 50% increase in the pseudo first order reaction rate (Fig. S5). Fig. 9b summarizes the relative electrocatalytic activities (expressed as $k_s^0$) of M–Sb–$SnO_2$ for EY, PhOH, and RNO with respect to those of Sb–$SnO_2$ (i.e., for substrate S, $k_s^0 = k_s$ at M–Sb–$SnO_2$/$k_S$ at Sb–$SnO_2$). Only Ni-doping enhanced the activity of all test substrates with the effect being most significant for PhOH ($k^0_{PhOH}$~8.5). The other anodes had selective activities depending on the substrates. For example, Ru, Co, and Pd doping enhanced the activity for EY ($k^0_{EY}$~1.5) but reduced it for RNO ($k^0_{RNO} < 1$), suggesting that these dopants might enhance the direct oxidation of EY at the anode surface via electron transfer. Fig. 9c shows the time-profiled changes in the RNO concentration at Ni–Sb–$SnO_2$ anodes as a function of the Ni doping levels. Ni doping of 0.5–2% increased the reaction rate by 30–55% as compared to Sb–$SnO_2$ whereas heavier doping reduced it. Fig. 9d compares the effects of Ni doping level on the $k_s^0$ values. Doping of Ni at 0.5–2% was optimal in enhancing the electrocatalytic activities of all test substrates. A further increase in the doping level reduced the activities, due likely to an increase in electrical resistivity or a change in the crystallinity of Sb–$SnO_2$. Nevertheless, the rates of PhOH and EY degradation were enhanced regardless of the Ni doping level.

Fig. 9d was re-plotted with $k^0_{RNO}$ vs. $k_s^0$ as a function of the Ni doping level, as shown in Fig. 10. The plots had no linearity, particularly because the data for Sb–$SnO_2$ (the cross between $k^0_{RNO} = 1$ and $k^0_S = 1$, where the number 1 refers to the value obtained at Sb–$SnO_2$) was out of range from the linear fashion. In addition, even if the data is excluded, the degree of enhancement for the substrates was far greater than those for RNO (i.e., $k^0_S/k^0_{RNO} \gg 1$; for example, $k^0_{PhOH}/k^0_{RNO}$~8.75). This means that the degradation rates of the substrates were enhanced, even though the rates for RNO were decreased at Ni–Sb–$SnO_2$. RNO has selective reactivity primarily with hydroxyl radicals and the reactivity with other species including singlet oxygen ($^1O_2$), peroxy radicals (•OOH or •OOR), hydroxyl radicals (•OH), and hydrogen peroxide ($H_2O_2$) were quite low [37,39,40]. Therefore, the kinetics shown in Fig. 10 strongly suggests that the improved electrocatalytic activity of Ni–Sb–$SnO_2$ should not be attributed to the enhanced generation of hydroxyl radicals. If this speculation is true, the absence of di-hydroxylated intermediates (catechol, hydroquinone, and resorcinol) and trace amounts of THB in the degradation of phenol at Ni–Sb–$SnO_2$ (Fig. 8) can be explained by direct oxidation, i.e., the direct electron transfer from substrates to the anodes (pathway 1 in Scheme 1). On the other hand, an alternative pathway involving hydrogen ozonide ($HO_3$•) can also be speculated. In this pathway, the competition

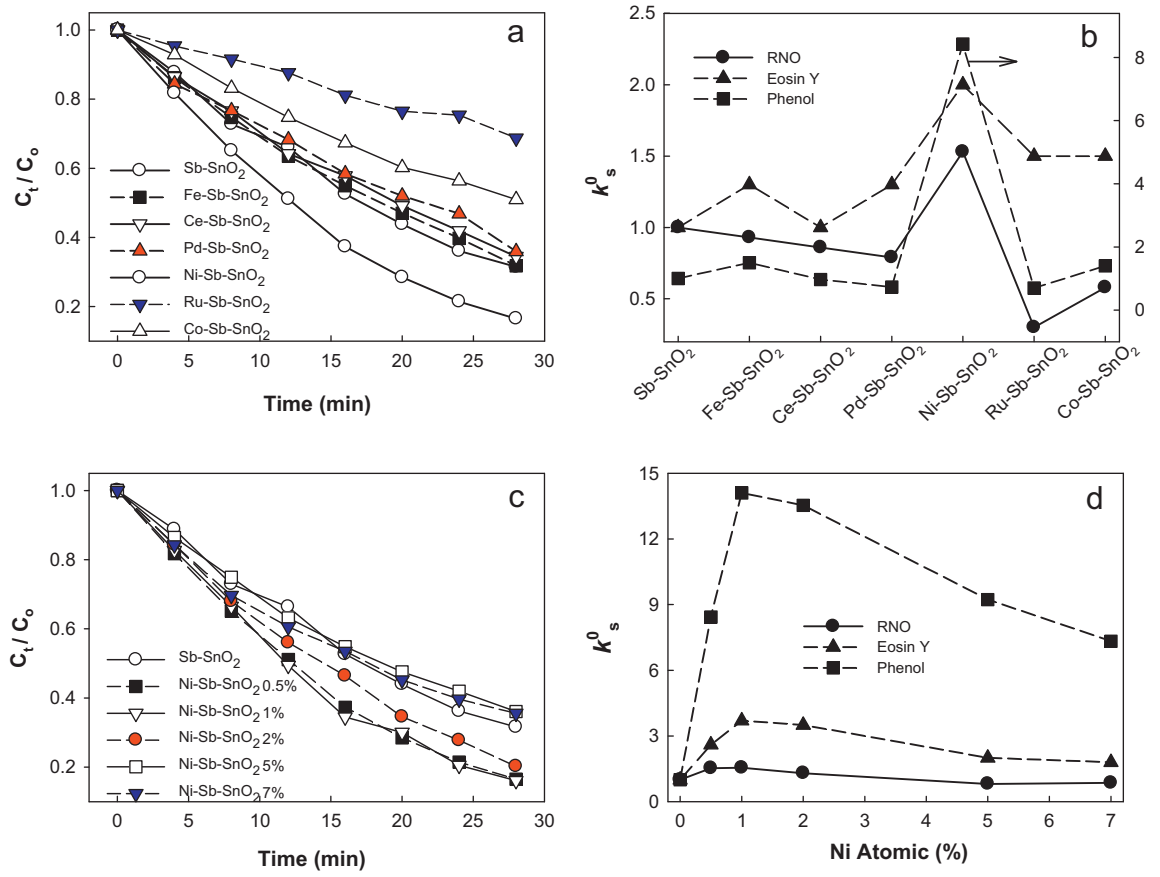


**Fig. 9.** (a and c) Time-profiled concentration changes of RNO at (a) M(0.5%)–Sb(5%)–$SnO_2$ and (c) Ni–Sb(5%)–$SnO_2$ anodes. (b and d) Comparison among the relative pseudo first order reaction rates ($k^0_S$) of Eosin Y, phenol, and RNO obtained at (b) M(0.5%)–Sb(5%)–$SnO_2$ and (d) Ni–Sb(5%)–$SnO_2$ anodes with respect to Sb(5%)–$SnO_2$ anode. $k^0_S = k_S$ at M–Sb–$SnO_2$/$k_S$ at Sb–$SnO_2$. $I$ = 0.1 A; $[RNO]_0$ = 1 mM; 0.1 M $Na_2SO_4$.

between the hydroxyl radical-mediated reaction (pathway 3) and the adsorption of dissolved oxygen molecules (pathway 4) may direct the reaction pathway afterward. If the latter is kinetically faster, then the formation of hydrogen ozonide will be favored, followed by ozone generation (pathways 5 and 6). On the other hand, Ni–Sb–$SnO_2$ was reported to be effective in generating ozone only in the absence and at very low concentrations of substrates, and no ozone was generated in the presence of substrates [26–28]. This suggests that the hydrogen ozonide might react with substrates (RH) forming organic peroxy radicals ($RO_2^{\bullet}$) that are responsible for the degradation of substrates (pathways 7 and 8). The insignificant reactivity of RNO with peroxy radicals may explain the improved electrocatalytic activity of Ni–Sb–$SnO_2$ for the substrates despite the reduced activity for hydroxyl radical-quenching RNO.

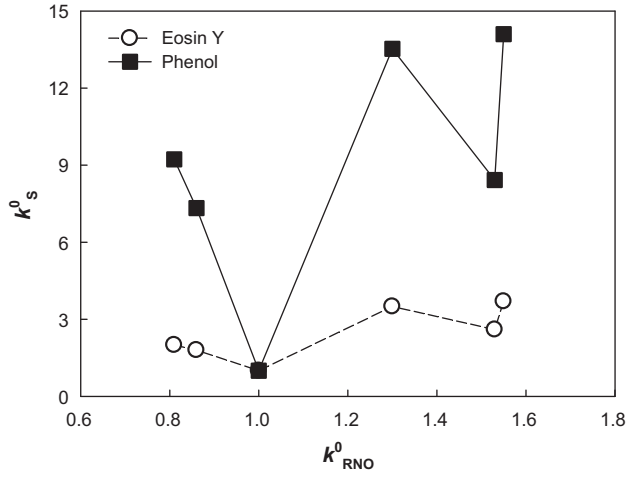


**Fig. 10.** Plots of $k^0_S$ vs. $k^0_{RNO}$ for Eosin Y and phenol. Data was taken from Fig. 9d (i.e., for Ni–Sb–$SnO_2$) and re-plotted.

## 4. Conclusions

This study examined the doping effects of metals on the electrochemical properties and electrocatalytic activities of $SnO_2$ and Sb–$SnO_2$ electrodes. The doping level of Sb in the Sb–$SnO_2$ electrode was optimal at 5–10%, and Ni and Fe enhanced the electrocatalytic activities of Sb(5%)–$SnO_2$. In particular, Ni was effective in boosting the activity of Sb–$SnO_2$ by a factor of 8–14 in terms of phenol degradation and by a factor of 7.7 in terms of the TOC removal efficiency. The lack of a correlation of the kinetics between RNO and other substrates (phenol and Eosin Y) suggests that the improvement by Ni doping might be attributed to the enhanced involvement of organic peroxy radicals. This result is significant, particularly in terms of crust abundance, because Fe and Ni are the most abundant metal elements of all the elements (8 elements including Sb and Sn) assessed in this study, promising wider application potentials of the electrodes.

## Acknowledgments

This study was supported by Basic Science Research Program (No. 2009-0071350, 2009-0089904, 2010-0002674, and

2011-0021148) and by the Korea Center for Artificial Photosynthesis (NRF-2009-C1AAA001-2009-0093879) through the National Research Foundation of Korea (NRF) funded by the Ministry of Education, Science and Technology.

## Appendix A. Supplementary data

Supplementary data associated with this article can be found, in the online version, at doi:10.1016/j.apcatb.2011.10.014.

## References

[1] O. Simond, V. Schaller, C. Comninellis, Electrochim. Acta 42 (1997) 2009–2012.
[2] M. Panizza, G. Cerisola, Electrochim. Acta 51 (2005) 191–199.
[3] B. Boye, M.M. Dieng, E. Brillas, Environ. Sci. Technol. 36 (2002) 3030–3035.
[4] Y.J. Feng, X.Y. Li, Water Res. 37 (2003) 2399–2407.
[5] M. Panizza, G. Cerisola, Chem. Rev. 109 (2009) 6541–6569.
[6] X.Y. Li, Y.H. Cui, Y.J. Feng, Z.M. Xie, J.D. Gu, Water Res. 39 (2005) 1972–1981.
[7] S. Tanaka, Y. Nakata, T. Kimura, Yustiawati, M. Kawasaki, H. Kuramitz, J. Appl. Electrochem. 32 (2002) 197–201.
[8] M. Li, C.P. Feng, W.W. Hu, Z.Y. Zhang, N. Sugiura, J. Hazard. Mater. 162 (2009) 455–462.
[9] S. Kim, S.K. Choi, B.Y. Yoon, S.K. Lim, H. Park, Appl. Catal. B: Environ. 97 (2010) 135–141.
[10] B. CorreaLozano, C. Comninellis, A. DeBattisti, J. Appl. Electrochem. 27 (1997) 970–974.
[11] M. Panizza, G. Cerisola, Appl. Catal. B: Environ. 75 (2007) 95–101.
[12] N.B. Tahar, A. Savall, J. Electrochem. Soc. 145 (1998) 3427–3434.
[13] J.M. Kesselman, O. Weres, N.S. Lewis, M.R. Hoffmann, J. Phys. Chem. B 101 (1997) 2637–2643.
[14] H. Park, C.D. Vecitis, W. Choi, O. Weres, M.R. Hoffmann, J. Phys. Chem. C 112 (2008) 885–889.
[15] H. Park, C.D. Vecitis, M.R. Hoffmann, J. Phys. Chem. A 112 (2008) 7616–7626.
[16] H. Park, C.D. Vecitis, M.R. Hoffmann, J. Phys. Chem. C 113 (2009) 7935–7945.
[17] H. Park, A. Bak, Y.Y. Ahn, J. Choi, M.R. Hoffmann, J. Hazard. Mater. (2011), doi:10.1016/j.jhazmat.2011.1005.1009.
[18] P. Canizares, F. Martinez, M. Diaz, J. Garcia-Gomez, M.A. Rodrigo, J. Electrochem. Soc. 149 (2002) D118–D124.
[19] R. Kotz, S. Stucki, B. Carcer, J. Appl. Electrochem. 21 (1991) 14–20.
[20] J. Kong, S. Shi, X. Zhu, J. Ni, J. Environ. Sci. 19 (2007) 1380–1386.
[21] D.L. He, S.I. Mho, J. Electroanal. Chem. 568 (2004) 19–27.
[22] Y.H. Cui, Y.J. Feng, Z.Q. Liu, Electrochim. Acta 54 (2009) 4903–4909.
[23] Y.J. Feng, Y.H. Cui, B. Logan, Z.Q. Liu, Chemosphere 70 (2008) 1629–1636.
[24] X.M. Chen, P.D. Yao, D.H. Wang, X.Z. Wu, Chem. Eng. J. 147 (2009) 412–415.
[25] M. Panizza, C. Bocca, G. Cerisola, Water Res. 34 (2000) 2601–2605.
[26] Y.H. Wang, S.A. Cheng, K.Y. Chan, X.Y. Li, J. Electrochem. Soc. 152 (2005) D197–D200.
[27] Q.Y. Chen, D.D. Shi, Y.J. Zhang, Y.H. Wang, Water Sci. Technol. 62 (2010) 2090–2095.
[28] Y.H. Wang, K.Y. Chan, X.Y. Li, S.K. So, Chemosphere 65 (2006) 1087–1093.
[29] C. Comninellis, Electrochim. Acta 39 (1994) 1857–1862.
[30] F. Montilla, E. Morallon, A. De Battisti, A. Benedetti, H. Yamashita, J.L. Vazquez, J. Phys. Chem. B 108 (2004) 5044–5050.
[31] F. Montilla, E. Morallon, A. De Battisti, S. Barison, S. Daolio, J.L. Vazquez, J. Phys. Chem. B 108 (2004) 15976–15981.
[32] C. Terrier, J.P. Chatelon, R. Berjoan, J.A. Roger, Thin Solid Films 263 (1995) 37–41.
[33] P. Yao, Desalination 267 (2011) 170–174.
[34] I.S. Mulla, H.S. Soni, V.J. Rao, A.P.B. Sinha, J. Mater. Sci. 21 (1986) 1280–1288.
[35] D.J. Goyal, C. Agashe, B.R. Marathe, M.G. Takwale, V.G. Bhide, J. Appl. Phys. 73 (1993) 7520–7523.
[36] Y.H. Cui, Y.J. Feng, J. Mater. Sci. 40 (2005) 4695–4697.
[37] G.V. Buxton, C.L. Greenstock, W.P. Helman, A.B. Ross, J. Phys. Chem. Ref. Data 17 (1988) 513–886.
[38] J.H. Grimm, D.G. Bessarabov, U. Simon, R.D. Sanderson, J. Appl. Electrochem. 30 (2000) 293–302.
[39] I. Kraljic, C.N. Trumbore, J. Am. Chem. Soc. 87 (1965) 2547–2550.
[40] D. Wabner, C. Grambow, J. Electroanal. Chem. 195 (1985) 95–108.